


## Characteristics of DC arcs in a multi-arc generator and their application in the spheroidization of $SiO_2$

Qifu Lin(林启富), Yanjun Zhao(赵彦君), Wenxue Duan(段文学), Guohua Ni(倪国华), Xinyue Jin(靳兴月), Siyuan Sui(隋思源), Hongbing Xie(谢洪兵), and Yuedong Meng(孟月东)

**Citation:**Chin. Phys. B, 2020, 29 (**12**): 125201. DOI: 10.1088/1674-1056/aba9
Journal homepage: http://cpb.iphy.ac.cn; http://iopscience.iop.org/cpb

**What follows is a list of articles you may be interested in**

---

## Characteristics of DC arcs in a multi-arc generator and their application in the spheroidization of $SiO_2$

Qifu Lin(林启富), Yanjun Zhao(赵彦君), Wenxue Duan(段文学), Guohua Ni(倪国华), Xinyue Jin(靳兴月), Siyuan Sui(隋思源), Hongbing Xie(谢洪兵), and Yuedong Meng(孟月东)
Chin. Phys. B, 2020, 29 (**12**): 125201. DOI: 10.1088/1674-1056/aba9

## Weakly nonlinear multi-mode Bell-Plesset growth in cylindrical geometry

Hong-Yu Guo(郭宏宇), Tao Cheng(程涛), and Ying-Jun Li(李英骏)
Chin. Phys. B, 2020, 29 (**11**): 115202. DOI: 10.1088/1674-1056/ab9c14

## Investigation on plasma structure evolution and discharge characteristics of a single-stage planar-pulsed-inductive accelerator under ambient fill condition

Xiao-Kang Li(李小康), Bi-Xuan Che(车碧轩), Mou-Sen Cheng(程谋森), Da-Wei Guo(郭大伟), Mo-Ge Wang(王墨戈), and Yun-Tian Yang(杨云天)
Chin. Phys. B, 2020, 29 (**11**): 115201. DOI: 10.1088/1674-1056/ab9f2a

## Effect of radio frequency bias on plasma characteristics of inductively coupled argon discharge based on fluid simulations

Xiao-Yan Sun(孙晓艳), Yu-Ru Zhang(张钰如), Sen Chai(柴森), You-Nian Wang(王友年), Yan-Yan Chu(楚艳艳), Jian-Xin He(何建新)
Chin. Phys. B, 2020, 29 (**9**): 095203. DOI: 10.1088/1674-1056/ab9436

## Experimental study on energy characteristics and ignition performance of recessed multichannel plasma igniter

Bang-Huang Cai(蔡帮煌), Hui-Min Song(宋慧敏), Min Jia(贾敏), Yun Wu(吴云), Wei Cui(崔巍), Sheng-Fang Huang(黄胜方)
Chin. Phys. B, 2020, 29 (**6**): 065207. DOI: 10.1088/1674-1056/ab820c

---

# Characteristics of DC arcs in a multi-arc generator and their application in the spheroidization of $SiO_2$*

Qifu Lin(林启富)[1,2], Yanjun Zhao(赵彦君)[1,2], Wenxue Duan(段文学)[1], Guohua Ni(倪国华)[1,3,†], Xingyue Jin(靳兴月)[1,2,3], Siyuan Sui(隋思源)[1,2], Hongbing Xie(谢洪兵)[1], and Yuedong Meng(孟月东)[1]

[1] *Institute of Plasma Physics, Chinese Academy of Sciences, Hefei* 230031, *China*
[2] *Science Island Branch of Graduate School, University of Science and Technology of China, Hefei* 230026, *China*
[3] *AnHui Province Key Laboratory of Medical Physics and Technology, Hefei* 230031, *China*

(Received 23 June 2020; revised manuscript received 20 July 2020; accepted manuscript online 28 July 2020)

We investigate characteristics of multi-arc torches with three pairs of electrodes (three cathodes and three anodes) and their performance on the spheroidization of $SiO_2$ powder. The effect of electrode arrangement, including adjacent pattern (AD pattern, adjacent electrodes powered by one power supply) and opposite pattern (OP pattern, opposite electrodes powered by one power supply), on the dynamics of arc plasma is investigated based on synchronous acquisition of electrical and optical signals. The results show that both the voltage and spatial distribution of each arc of multiple arcs are more stable compared with those of a single arc. The fluctuation of an arc in multiple arcs mainly comes from the small-scale arc-to-arc restrikes among multiple arcs. Moreover, these arc-to-arc restrikes occur more frequently among multiple arc columns in OP pattern than in AD pattern. Moreover, the high-temperature area of the central region of arc chamber in OP pattern is larger than that in AP pattern. For the spheroidization of $SiO_2$ in this multi-arc generator, the spheronization degrees of plasma treated silica in OP pattern are at least 20% higher than those in AD pattern.

**Keywords:** characteristics, multiple arcs, arc volume, spheroidization

**PACS:** 52.80.Mg, 52.70.–m, 52.50.Dg, 52.30.–q **DOI:** 10.1088/1674-1056/ab9de9

## 1. Introduction

Arc thermal plasmas have drawn extensive attention for their unique features, such as high temperature, high-energy density and high activity. They have been widely used in the industrial field, such as metal cutting,[1,2] preparation of spherical powder,[3–5] thermal plasma spray,[6,7] solid hazardous wastes treatment,[8,9] and nanoparticles synthesis.[10,11] However, it should be noted that some of the characteristics of arcs may be positive for one specific application, while those may be negative for other applications. For instance, due to self-induced magnetic compression and thermal-pinch effect,[12–14] the energy of an arc is mainly concentrated in the arc column, and its radial dimension is very small, which is very suitable for metal cutting.[1,2] However, this characteristic is disadvantageous to material processing, such as powder spheroidization[3–5] and thermal spray,[6,7] since it is difficult for particles to fully enter the arc column owing to its small size. Therefore, it is necessary to regulate arc plasmas to obtain the best performance according to specific applications, in order to meet the needs of actual industrial applications.

There are several ways to enlarge an arc plasma volume to meet its applications in various fields,[15–27] including coal pyrolysis,[17,18] preparation of glass,[19–21] thermal spray[22,23] and spheroidization of alumina powder.[24,25] Unlike conventional linear plasma torches, a V-type plasma torch can produce two separate arc columns, cathode arc column (CAC) and anode arc column (AAC).[17,18] A large area of high temperature is formed at the junction of CAC and AAC, and therefore the acetylene yield has been improved when the coal powder was injected into this thermal plasma reactor.[17,18] The use of multi-phase AC arc torch can also achieve the purpose of expanding the high-temperature region of arc plasma.[19–21,26,27] The initial multi-phase AC arc torch was powered by a 3-phase power supply.[26,27] Although the high-temperature region is expanded in this 3-phase arc torch, there are significant differences among the discharge intensities of multiple arcs due to low frequencies of arc currents causing the remarkable phase transition, which results in the intermittent discharge and arc instability. In order to improve performance of a 3-phase arc plasma, a new multi-phase arc generator with multiple electrodes powered by a 6-phase or 12-phase AC power supply has been developed, and used for the preparation of glass.[19–21] Compared with the 3-phase arc discharge, the problem of intermittent discharge has been effectively improved for both the 6-phase and 12-phase arc plasmas. Moreover, by increasing the phase number of power supply from 6 to 12 phases, the size of a multi-phase arc plasma was expanded, and thus larger space and longer residence time are allowed for the effective heating of raw glass powders. However, the arc fluctuation from the intermittent discharge cannot be thoroughly resolved

*Project supported by the National Natural Science Foundation of China (Grant Nos. 11875295 and 11535003), the National Key R&D Program of China (Grant No. 2019YFC0119000), Provincial Science and Technology Major Project of Anhui Province, China (Grant No. 17030801035), and Key Program of 13th Five-Year Plan, CASHIPS, China (Grant No. KP-2017-25).

†Corresponding author. E-mail: ghni@ipp.ac.cn

© 2020 Chinese Physical Society and IOP Publishing Ltd 

in multi-phase AC-driven arc torch. An alternative method of enlarging the high-temperature region of arc plasma is multiple electrode plasma torch driven by direct current. Schein *et al.*[22] have designed a multi-arc generator with three anodes and one common cathode (DeltaGun) or three cathodes and one common anode (TRIPLEX) for the application of thermal spray. In these multi-electrode plasma torches, a high-temperature zone with lower viscosity surrounded by three arc columns can be generated, which enables better entrainment of the particles into the jet core and thus achieves particles better molten. In order to further enlarge the arc volume in a DC multi-arc generator, regulating the spatial distribution of arc plasma to make multiple arcs more diffuse may be a good choice. Wang *et al.*[24,25] has invented a diffuse arc plasma source by means of a multi-arc generator with six cathodes and a common anode working with helium/argon mixture medium. With the increasing of helium content in helium/argon mixture, the uniformity and stability of diffuse arc plasma were enhanced. The large-size diffuse arc plasma and long plasma jet provided uniform and stable condition for the spheroidization of alumina powder.

In the present work, a DC multi-arc generator with three pairs of electrodes driven by three separate power supplies is developed and used to spheroidize $SiO_2$ powder. According to the connection sequence between electrodes and power supplies, two typical electrode arrangements are established. The effect of electrode arrangement on the dynamics of arc plasma, arc stability and spatial distribution is investigated via analyzing the arc voltage and discharge images collected synchronously. Then, the silicon raw materials are processed in the multi-arc generator with different configurations, and the corresponding spherodization performances of $SiO_2$ powders are compared and analyzed.

## 2. Experimental setup

The schematic diagram of the experimental setup is presented in Fig. 1. It mainly includes a multi-arc generator, a feed gas system, three identical power supplies, and the measurement and diagnosing system. The multi-arc generator mainly consists of three pairs of electrodes and an arc chamber. Each one of these electrodes was thoriated tungsten copper rod with 11 mm in diameter and cooled by cooling water, and was insulated by respective concentric ceramic bushings with an inner diameter of 31 mm. A ring was used to form swirling gas in the gap between electrode and bushing. These electrodes were radially inserted into the arc chamber with inner diameter of 100 mm, and the distance of every two opposite electrode tips was about 50 mm. Six electrodes were classed into three pairs, and each pair of electrodes containing one anode and one cathode were connected to the positive and negative output of a DC power supply, respectively. All the positive outputs were not grounded. Two connection types between electrodes and power supplies were employed: adjacent (AD) pattern and opposite (OP) pattern, as shown in the upper left corner of Fig. 1. In AD pattern, the cathode and anode of each pair of electrodes were arranged adjacent to each other. In OP pattern, the cathode and anode of each pair of electrodes were disposed opposite to each other. The plasma working gas was pure argon gas, which was injected into the gap between electrode and bushing. The direction of plasma working gas was in straight flow at the exit of electrode, and the gas flow rate of each electrode was 2 $m^3$/h. The multi-arc generator was powered by three power supplies with each one allowing the maximum no load output voltage of 200 V and adjustable output current from 0 to 600 A. The default discharge current of each arc was 120 A unless the discharge power needed to be changed.

A high-speed CCD camera (Vision Research, Inc., Phantom v711) was utilized to record the discharge image of multiple arcs under the condition of a frame rate of 30000 fps (frames per second) and an exposure time of 0.02 ms. In order to prevent the overexposure of discharge image, a narrowband filter of 416 nm was placed in front of the lens of CCD camera. The captured discharge image had a resolution of 256×256 pixels and gray-value range of 0–255. The electrical potentials of the six electrodes were measured using two four-channel oscilloscopes (KEYSIGHT DSOX2024A) with six voltage probes (KEYSIGHT N2862B). A trigger equipment was employed to synchronically collect the arc discharge voltages and discharge images.

A powder feeder (Tekna Plasma System Inc., PFD402-FM) was employed to carry the raw irregular silica powder (Nanjing Mingshan New Material Co., Ltd., China) into the discharge zone. The argon carrier gas flow of powder feeder was set at 5 slm (standard liter per minute). The powder feed rate was selected to be 5.6 g/min. The powder feed nozzle with an inner diameter of 3 mm was fixed at the position with a distance of 20 mm above the plane formed by six electrode tips. During the processing of silica powders, the upper end of arc chamber was covered by a circular lid with a central hole allowing the powder feed nozzle passing through, and the powder processed was collected by a glass container filling with water.

To evaluate the spheroidization rate of silica powders processed by the multi-arc plasma, the optical microscopy (SMM-3300C, Shuyao, China) was utilized to count the total number of powders and the amount of spherical powders in the optical microscopy images. The particle morphology of silica powders before and after processing was observed by a scanning electronic microscope (SEM, ZEISS GeminiSEM 500, Germany), and the particle phase was characterized by x-ray diffraction (XRD, X'Pert MPD Pro, Philips, The Netherlands) using nickel-filtered Cu $K\alpha$ radiation (30 kV, 30 mA).

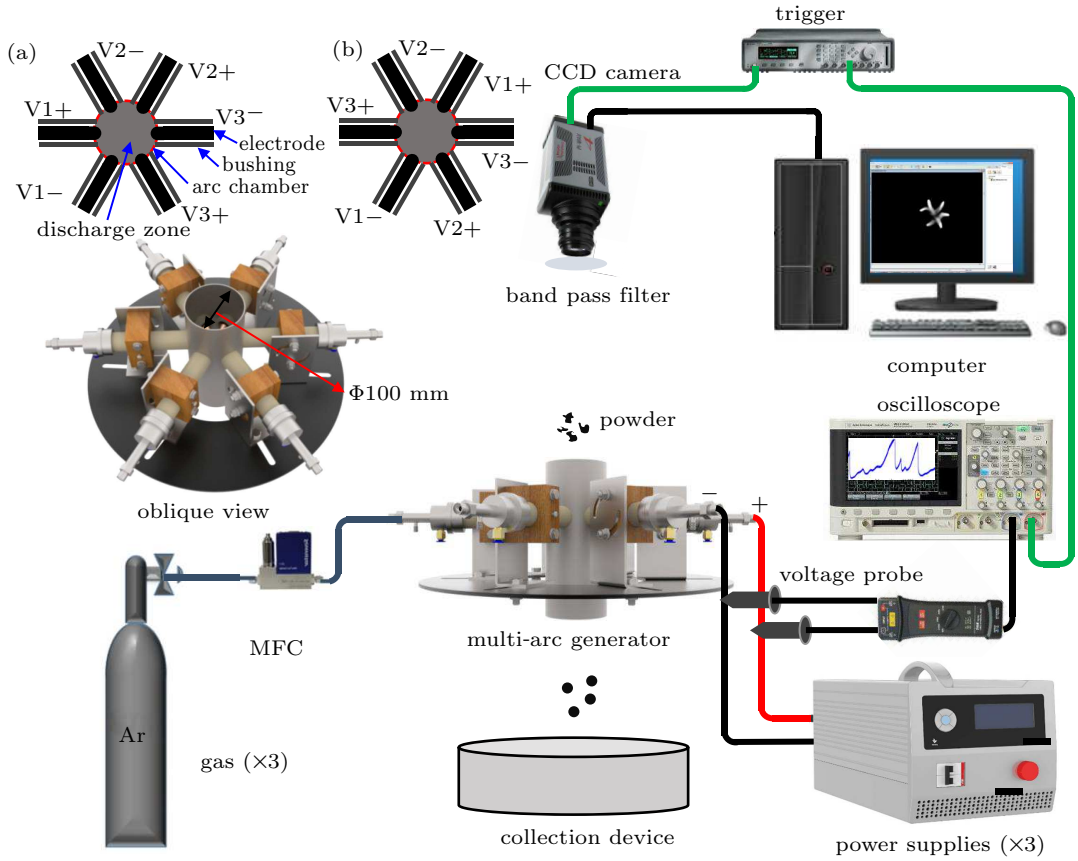



**Fig. 1.** Experimental setup in the multi-arc generator and two typical electrode arrangements in the upper left corner with (a) adjacent pattern and (b) opposite pattern.

## 3. Results and discussion

### 3.1. Typical discharge image in the multi-arc generator

For comparison, the dynamics of single-arc and multi-arc discharges were investigated in the experiment. The multi-arc generator can operate in both single-arc mode and multi-arc mode, which was implemented by means of controlling the amount of power on. Figure 2 shows the typical discharge images for single and multiple arcs in AD and OP patterns. As it can be seen in Figs. 2(a) and 2(b), the shape of arc column was V-type both for single arc and each one of multiple arcs in AD pattern. The arc column for a single arc almost passed through the whole arc chamber, while each arc in multiple arcs was constrained in relatively small region in AD pattern. In addition, each arc in multiple arcs connected with other arcs in the center of arc chamber, which may create branch current of the arc column. In OP pattern, the arc column for single arc had a Z-type as shown in Fig. 2(c), while the shape of multiple arcs was similar to that in AP pattern, as shown in Fig. 2(d). Furthermore, it was worth noting that a CAC driven by one power supply was mainly connected to the AAC driven by another power supply, which appeared to form a complete arc, in both AD and OP patterns of the multi-arc system. Owing to this particular connection among multiple arcs, it can be speculated that the arc current mainly flows from V1+, V2−, V2+, V3−, V3+ to V1−, as shown in Fig. 2(b). This indicated that these arcs both in AD and OP pattern were chained together to form a whole. In order to more clearly understand the whole current direction both inside the arc channel and driving power supply, the equivalent electrical circuit schematic for the equivalent electrical model of multiple arcs in AD pattern and the related circuit of power supply is shown in Fig. 3. It can be observed that three arcs and their driving power supplies composed a whole closed current loop. Actually, in addition to the main connection paths mentioned above, there were other weak connection paths between arc columns, and therefore multiple arcs were connected by complex series-parallel.

The particular connection order between arcs with a CAC driven by one power supply mainly connected to the AAC driven by another power supply in multi-arc system may be mainly related to the slightly asymmetry distribution of six electrodes. Taking AD pattern as the example, due to the machining accuracy of arc chamber, the distance (the total distance from two electrode tips to the intersection point of their axis lines) between electrode V1+ and electrode V2− was slightly shorter than that between electrode V1+ and electrode V1−. Therefore, the arc current would flow from electrode V1+ to electrode V2− rather than electrode V1−.

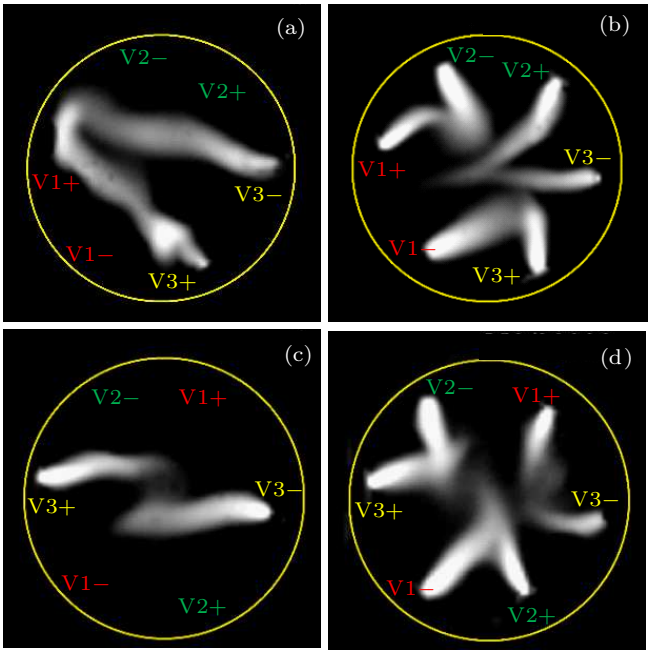



**Fig. 2.** Typical discharge image in multi-arc generator for (a) single arc in AD pattern, (b) multiple arcs in AD pattern, (c) single arc in OP pattern, (d) multiple arcs in OP pattern.

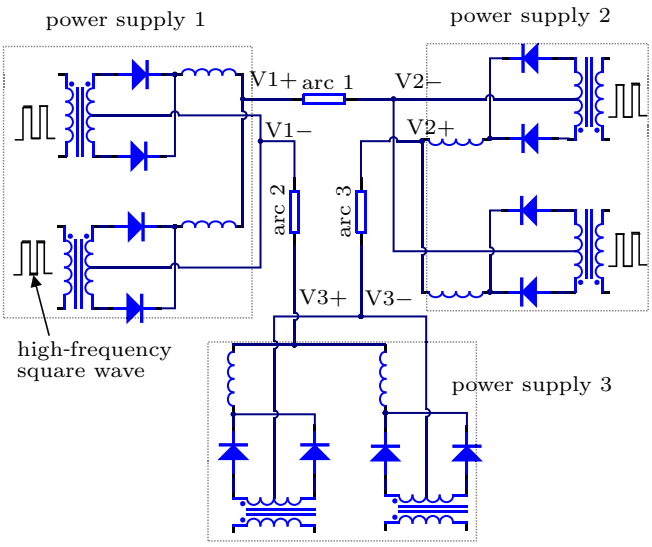



**Fig. 3.** The equivalent electrical circuit schematic between power supplies and multiple arcs in AD pattern.

### 3.2. Temporal and spatial evolutions of arc discharge

The temporal and spatial behaviors of arc columns in the multi-arc generator were investigated by means of simultaneous signal collection of the discharge image and arc voltage. For analysis and comparison conveniently, the behaviors of a single arc generated in the multi-arc generator were also investigated in the experiment. Figure 4 presents the successive discharge images and arc voltage waveform acquired in synchronization for a single arc and multiple arcs in AD pattern. As seen in Fig. 4(a), the arc column for the single arc in AD pattern was elongated at irregular intervals inside the arc chamber. In addition, the elongation direction of arc column varied in different regions of arc chamber, which is associated with gas flow field in arc chamber. The magnitude and direction of gas-flow velocity has remarkable difference in different regions of the arc chamber, which is caused by the stronger offset of six gas sources coming from six electrodes with the position closer to the center of the arc chamber. That is to say, there was a region with low gas-flow velocity in radial direction of arc chamber and high gas-flow velocity in axial direction formed in the center of the arc chamber. During the elongation of arc column, large-scale arc-to-arc restrike occurred, which resulted in a dramatic variation of arc voltage. However, once three arcs simultaneously appeared in the arc chamber, each one of multiple arcs in AD pattern would become relatively more stable during the successive evolution of arc discharge, as shown in Fig. 4(b). The reason of this phenomenon may be associated with the forces applied on the arc column. For each one of multiple arcs,[28–30] the Lorentz forces originating from the other two arc columns act on this arc column in the opposite direction of gas drag force, which would be favor for the balance of resultant force acting on arc column. As can be seen from the voltage waveform collected synchronously in Fig. 4(b), the fluctuation of each arc voltage included small-scale low-frequency fluctuation (LFF) and high-frequency fluctuation (HFF).

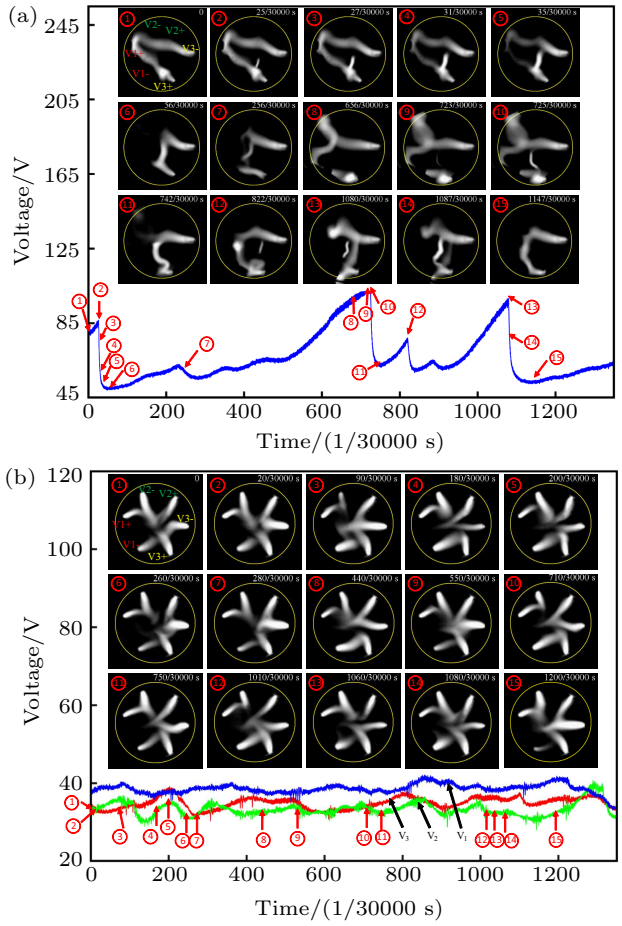



**Fig. 4.** The arc voltage and sequential arc discharge images for (a) single arc and (b) multiple arcs in AD pattern. The $V_1$, $V_2$, and $V_3$ represent the arc voltages between electrodes V1+ and V1−, V2+ and V2−, V3+ and V3−, respectively.

Both of these arc fluctuations appeared to follow no discernible cycle. The duration of each fluctuation for these small-scale LFF and HFF was on the order of sub-milliseconds and microseconds, respectively. The fluctuation magnitudes for LFF and HFF were mainly in the range of around 0–10 V and 0–3 V, respectively. The LFF may be mainly associated with the slight variation of arc connection order as shown in Fig. 4(b), which results in the slow variation of arc length and voltage. In addition, the slow arc elongation as shown in Fig. 4(b) also resulted in the slow variation of arc length and voltage. For the HFF, it may be caused by the arc-to-arc restrike among multiple arcs, which resulted in generation of a new co-existing arc branch. In the process of multiple arc operation, the spacing between arc columns changed frequently and decreased in the central region of the arc chamber due to the movement of arcs, which made it easy for two points located on the respective cathode and anode arc column to meet the requirement of gas breakdown. As a result, the small-scale arc-to-arc restrike between arc columns would occur frequently, and this could result in many high frequency burrs contained in the arc voltage waveform.

Figure 5 presents the successive discharge images and arc voltage for a single arc and multiple arcs in OP pattern under the same experimental condition mentioned above. For the single arc and the multiple arcs in OP pattern as shown in Fig. 5, the arc shape and length were relatively stable. Correspondingly, arc voltage changed slowly and slightly, and arcs were constrained within a relatively small range. However, there was much stronger HFF in arc voltage for multiple arcs than that of the single arc. In addition, the arc connection among multiple arcs in OP pattern seemed to be more frequent compared with that in AD pattern, which suggests that the occurrence of small-scale arc-to-arc restrikes in OP pattern may be more frequent. Therefore, the corresponding arc voltage in OP pattern had greater HFF.

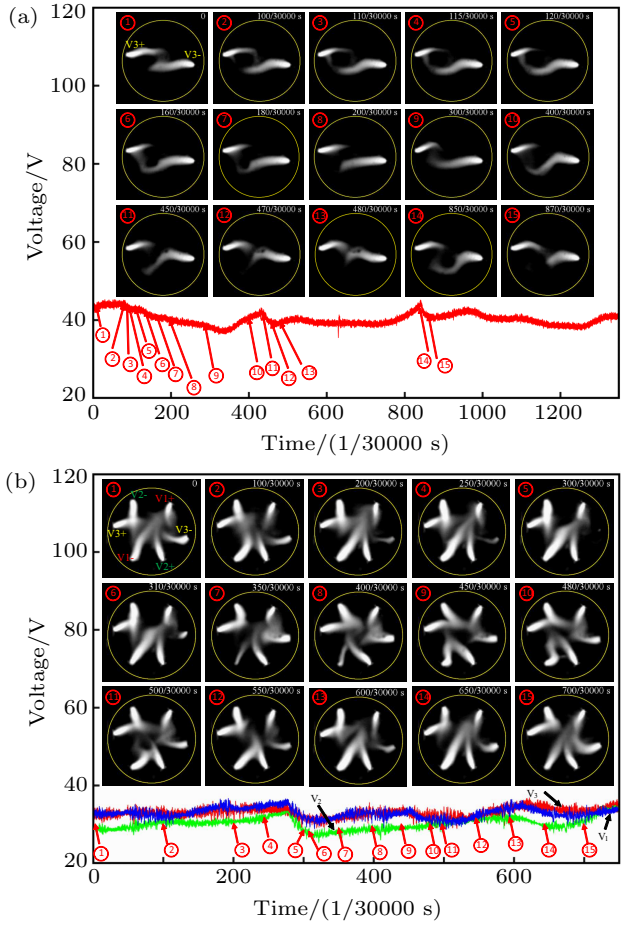



**Fig. 5.** The arc voltage and sequential arc discharge images for (a) single arc and (b) multiple arcs in OP pattern.

### 3.3. Fluctuation of arc voltage

In order to quantitatively analyze the arc stability,[31–33] statistical analysis was employed to obtain the mean, standard deviation, and cross-correlation coefficient of arc voltages for multiple arcs in AD and OP patterns as shown in Table 1. There was no significant difference between the mean arc voltage of AD and OP patterns. The standard deviation of arc voltage both in AD and OP patterns was relatively small. Therefore, the fluctuation behavior for multiple arcs both in AD pattern and OP pattern was characterized by small-scale arc fluctuation.

Owing to arc connection resulting in the interconnectedness among multiple arcs, the fluctuations of arc voltage among multiple arcs may have a certain degree of synchronism, which can be quantitatively represented by the coefficients of cross-correlation analysis.[31] By means of the cross-correlation analysis among multiple arc voltages, it was found that the cross-correlation coefficients among multiple arc voltages in AD pattern were 0.27, 0.38 and 0.41, respectively, while in OP pattern these values were 0.30, 0.39 and 0.50, respectively, as listed in Table 1. The correlation degree among multiple arcs in OP pattern is higher than that in AD pattern. The higher correlation degree among multiple arc voltages means a larger share for the synchronous fluctuation in the whole fluctuation of arc voltages. Therefore, it can be inferred that more frequent arc-to-arc restrikes occurred in OP pattern, which is consistent with the result mentioned in section 3.2.

**Table 1.** Statistic analysis of arc voltage for multiple arcs in AD and OP patterns.

| Plasma type | Mean arc voltage/V | Standard deviation of arc voltage/V | Cross-correlation coefficient among multiple arc voltages |
|---|---|---|---|
| Multiple arcs in AD pattern | 34.81; 33.32; 38.44 | 1.67; 1.82; 1.55 | 0.27; 0.38; 0.41 |
| Multiple arcs in OP pattern | 33.46; 31.62; 32.93 | 1.53; 2.22; 1.38 | 0.30; 0.39; 0.50 |

To identify the origination for the fluctuation of arc voltage by frequency domain, the fast Fourier transform (FFT) method was employed to calculate the power spectra of arc voltages for multiple arcs in both AD and OP patterns as presented in Fig. 6. The prominent peaks situated at 37 kHz and 74 kHz were clearly visible in all spectra, which were originated from the output undulation of power supply. In our experiment, it was found that most of the frequency spectra for single arc and multiple arcs in AD pattern were similar, but the frequency band of 1–25 kHz only appeared in the power spectra of multiple arc voltages. Thus it can be inferred that the unique frequency band of 1–25 kHz for multiple arcs may originate from the occurrence of arc-to-arc restrike among multiple arcs, which results in the HFF in arc voltage waveform. The amplitude of frequency band of 1–25 kHz for multiple arcs in OP pattern was obviously larger than that in AD pattern, which implies that the occurrence of arc-to-arc restrike in OP pattern was more remarkable. In addition, there was also low-frequency band of 0.05–1 kHz appearing in the spectra, which may be caused by the slight variation of arc connection order and slow arc elongation.

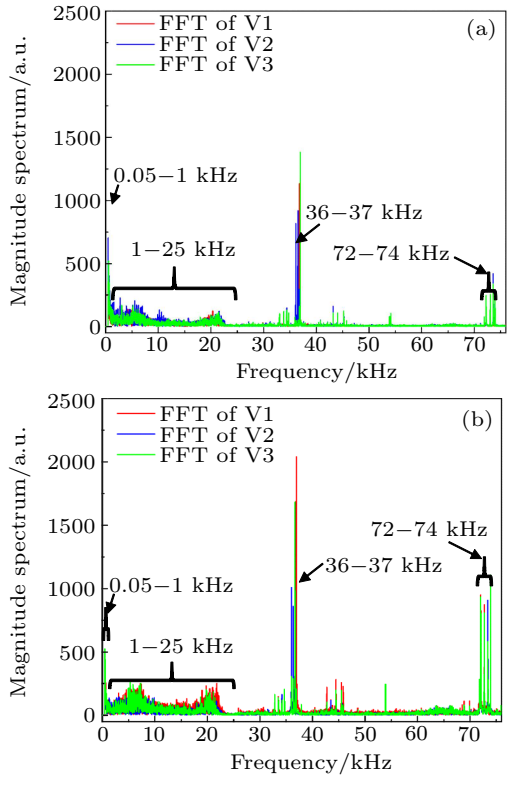



**Fig. 6.** The FFT spectra of arc voltage waveform for (a) multiple arcs in AD pattern and (b) multiple arcs in OP pattern.

In order to track the occurrence time of the FFT spectra as mentioned above, the time-frequency analysis was employed to process the arc voltage signal. The calculation method of time-frequency analysis selected the short-time Fourier transform (STFT). Figure 7 displays the STFT distribution of arc voltage signal for multiple arcs in AD and OP patterns. The frequency band of 1–25 kHz for multiple arcs in time domain was discrete unlike the continuous spectra of 37 kHz and 74 kHz caused by the output undulation of power supply. Since the occurrence time of arc-to-arc restrike was intermittent, the corresponding time-frequency spectra caused by arc-to-arc restrike were discrete. Therefore, this result further verified that the frequency band of 1–25 kHz for multiple arcs originates from the occurrence of small-scale arc-to-arc restrikes.

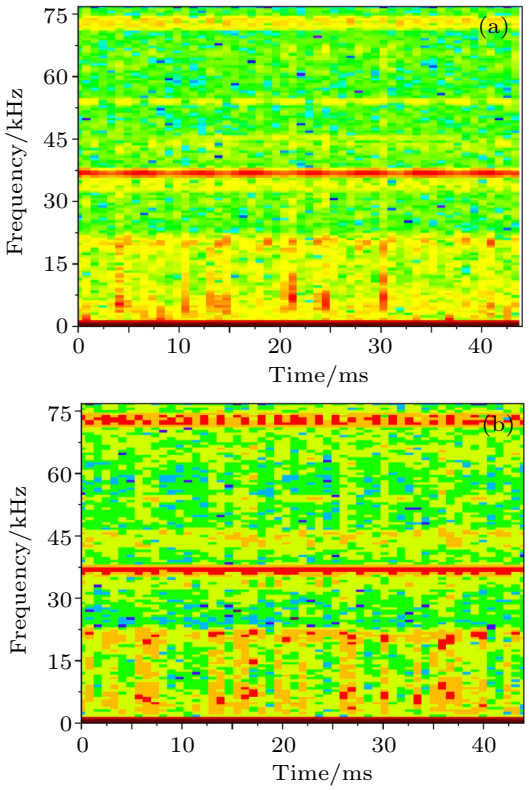



**Fig. 7.** The short-time Fourier transform (STFT) spectra of arc voltage waveform for (a) multiple arcs in AD pattern; (b) multiple arcs in OP pattern.

### 3.4. Arc spatial distribution and its fluctuation

The region covered by arc plasma or high temperature can be represented by the luminance area of discharge image.[20,21] To obtain the luminance area, the processing method refers to the literature,[34–36] which was derived from averaging the successive multiple discharge images at each pixel. The number of discharge image processed was selected as 3000 and 10000, whose time scale was around sub-millisecond. This time duration was roughly in consistence with the residence time of powder particle in the arc chamber. Figure 8 presents the average spatial distribution of luminance area in AD and OP patterns for different numbers of frame images. It can be observed that the luminance area in OP pattern was obviously larger than that in AD pattern as shown in Figs. 8(a) and 8(c), which suggests that the mean spatial distribution of arc plasma

is relatively more dispersed in OP pattern. The reason for this phenomenon may be related to the dynamic behavior of multiple arcs, especially the arc-to-arc restrike. The new arc-to-arc restrike in the center of arc chamber means the establishment of new arc channel, and thus the cold gas in the region covered by new arc channel was efficiently heated. The more frequent and random arc-to-arc restrikes in OP pattern result in the fact that more cold gas in different regions of the arc chamber was heated rather than the gas in certain small region. Further, there was no distinguishable difference for the average spatial distribution of luminance area between 3000 and 10000 frame images processed both in AD and OP patterns as shown in Fig. 8, which implies that the spatial distribution of arc plasma was relatively stable at the time scale of milliseconds.

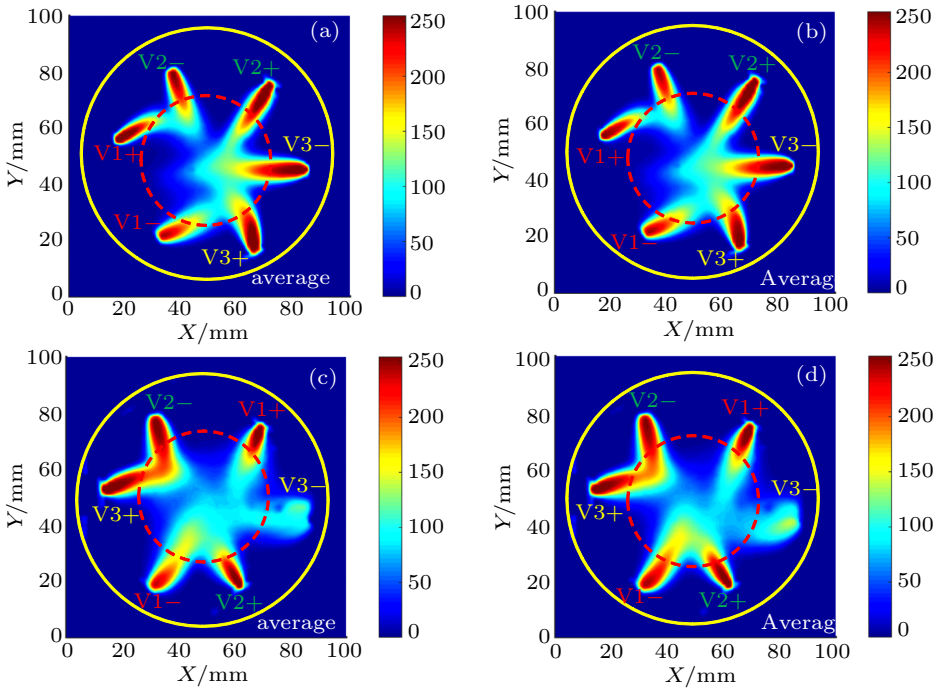



**Fig. 8.** The average spatial distribution of gray value of discharge image in multi-arc generator with AD pattern under (a) 3000 frames processed and (b) 10000 frames processed, and with OP pattern under (c) 3000 frames processed and (d) 10000 frames processed. The red circle in the figure represents the central region of the arc chamber.

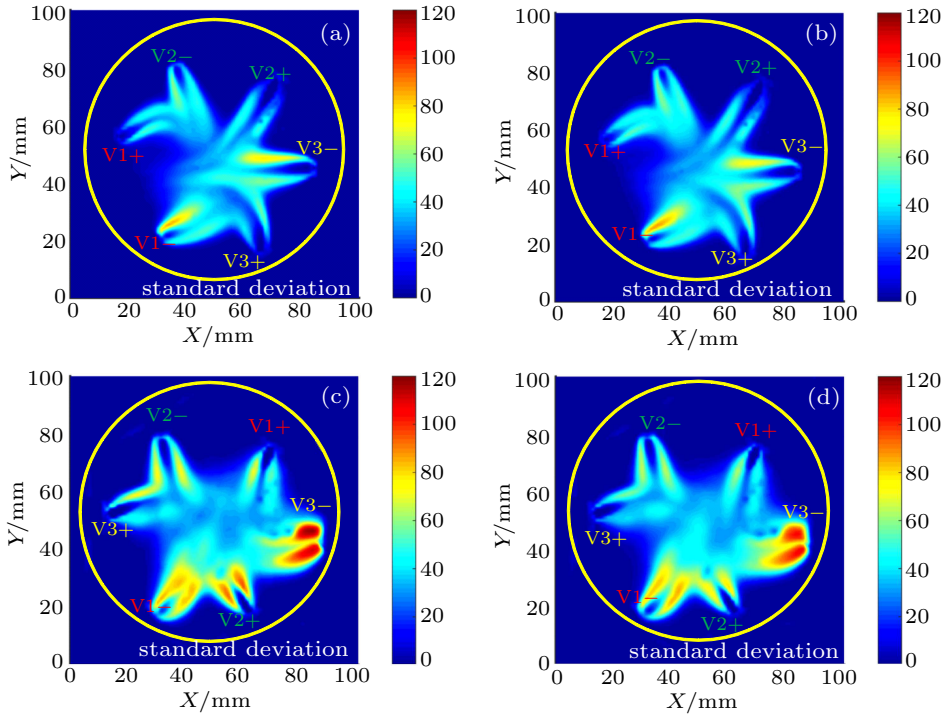



**Fig. 9.** The standard deviation distribution of gray value of discharge image in the multi-arc generator with AD pattern under (a) 3000 frames processed and (b) 10000 frames processed, and with OP pattern under (c) 3000 frames processed and (d) 10000 frames processed.

The spatial fluctuation of arc plasma distribution is an important parameter evaluating the application potential of arc plasma. By means of standard deviation analysis on the discharge image,[34–36] figure 9 presents the standard deviation of spatial distribution of arc discharge in AD and OP patterns for different numbers of processed frame images. The fluctuation degrees of arc spatial distribution both in AD and OP patterns were relatively smaller in the center of discharge zone. However, the whole fluctuation area of arc spatial distribution in OP pattern was larger than that in AD pattern, which is consistent with the more frequent formation of arc-to-arc restrike among multiple arcs in OP pattern. Combined with the effect of electrode arrangement on the luminance area mentioned above, it can be concluded that the electrode arrangement has great effect on the spatial distribution of multiple arcs and its temporal-spatial stability in the multi-arc generator.

### 3.5. Spheroidization of silica powder

To further verify the effect of electrode arrangement on the spatial distribution of arc plasma in the multi-arc generator, a series of experiments for the spheriodization of silica powder were conducted. Figure 10 presents the SEM images of silica powder before and after the plasma processing in AD and OP patterns. The raw powder particles were irregularly shaped, and the particle size varied from 7 μm to 65 μm. After the plasma processing, the shapes of many powder particles became spherical. The particle size increased and ranged from 10 μm to 85 μm. In addition, the spheroidization rate of $SiO_2$ seemed to be higher in OP pattern than that in AD pattern.

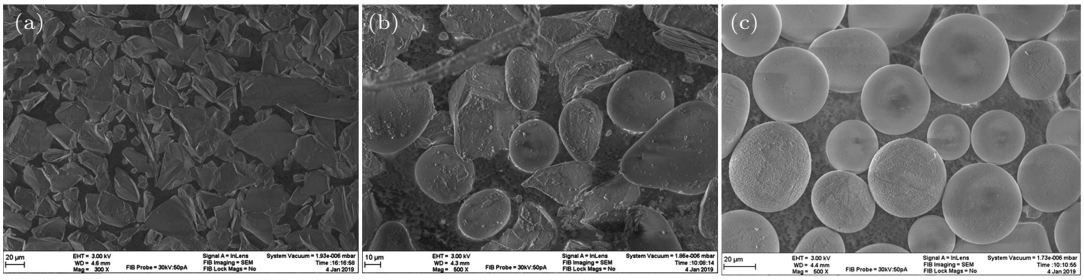



**Fig. 10.** SEM images of silica powder under different processing for (a) unprocessed silica powder, (b) the plasma-processed ones in AD pattern, and (c) the plasma-processed ones in OP pattern.

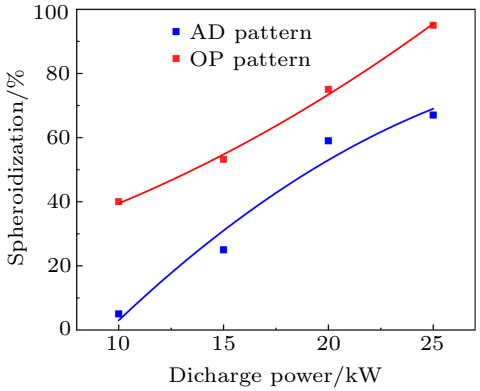



**Fig. 11.** Spheroidization rate of silica powder in multi-arc generator as a function of discharge power in AD and OP patterns.

By means of statistic of optical images, the effect of electrode arrangement on the spheroidization rate under different discharge powers is shown in Fig. 11. It can be clearly seen that a larger discharge power resulted in a higher spheroidization rate of $SiO_2$. The spheroidization rate of $SiO_2$ in OP pattern increased by at least 20% compared with that in AD pattern. The spheroidization rate reached to approximately 95% at a discharge power of 25 kW in OP pattern. In a given plasma torch, the critical parameter of affecting the spheroidization rate was the size of the high-temperature area of the arc chamber, which determined the ability of spheroidization processing. Therefore, the result of better spheroidization performance in OP pattern was consistent with the larger high-temperature area in OP pattern as mentioned in the above section. It can be concluded that electrode arrangement has a great effect on the spheroidization effect, and multi-arc generators with OP pattern may be more suitable for the spheroidization.

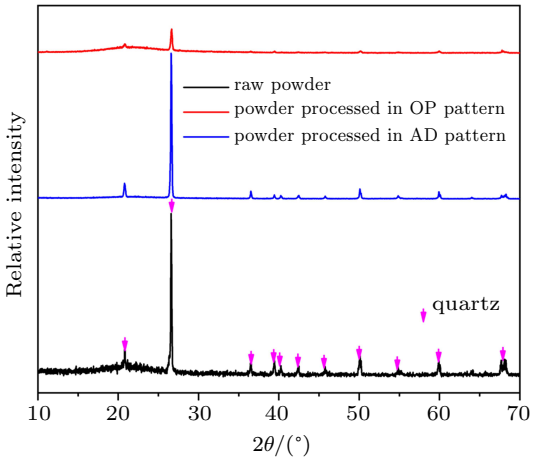



**Fig. 12.** XRD spectra of raw silica powder, and processed after plasma in AD and OP patterns.

The chemical elements and inner crystal structure of $SiO_2$ were other parameters for evaluating the spheroidization effect by plasma processing. In order to clarify the crystal phase and purity of $SiO_2$, XRD analyses were implemented. The XRD spectra of unprocessed silica powder and the plasma-

processed ones under AD and OP patterns are shown in Fig. 12. It can be observed that the XRD patterns of the unprocessed silica powder were characterized by diffraction peaks of quartz, which corresponds to the hexagonal $SiO_2$ (JCPDS card No. 46-1045). The diffraction peaks of quartz became more pronounced for the silica powder processed in AD pattern, while these diffraction peaks almost disappeared for the silica powder processed in OP pattern. This result indicates that the transition of powder phase from quartz phase to an amorphous one occurs when the multi-arc generator operated from AD pattern to OP pattern. Furthermore, all the diffraction peaks of quartz were assigned to the hexagonal $SiO_2$ structure, which suggests that there were no impurities incorporated in the powder after plasma processing in our device. The crystallite diameter of the quartz structure can be calculated using the Scherrer equation.[37] As listed in Table 2, the crystalline size of silica powder processed by arc plasma decreased compared with that of the raw ones.

**Table 2.** Comparison of the crystal cell parameters of silica powder before and after plasma processing.

| Powder type | Space group | Crystal parameters | | | Crystalline size/nm |
|---|---|---|---|---|---|
| | | *a*/Å | *b*/Å | *c*/Å | |
| Raw powder | Hexagonal | 49.13 | 49.13 | 54.05 | 61.48 |
| Powder processed in AD pattern | Hexagonal | 49.13 | 49.13 | 54.05 | 52.74 |
| Powder processed in OP pattern | Hexagonal | 49.13 | 49.13 | 54.05 | 36.00 |

## 4. Conclusion

In summary, a multi-arc generator with three pairs of electrodes powered by three independent DC power supplies has been developed to obtain large-scale arc plasmas at atmospheric pressure. The effect of electrode arrangement including AD and OP patterns on the dynamics of arc plasmas, the arc stability, and the spatial distribution of arc plasmas is investigated. Then, the spheroidization of $SiO_2$ was performed in this multi-arc generator. Conclusions drawn from the experimental results and analyses of arc behaviors are listed as follows.

The multi-arc shape presents three V-type arc columns in multi-arc generator both for AD and OP pattern. Compared with single arc, each of multiple arcs is more stable. The fluctuation of multiple arcs mainly comes from small-scale arc-to-arc restrikes. Moreover, the arc-to-arc restrike is more frequent in OP pattern than that in AD pattern. In addition, the arc-to-arc restrikes result in the interconnectedness among multiple arcs, and thus a larger share appears for the synchronous fluctuation in the whole fluctuation of arc voltages in OP pattern than in AD pattern.

The mean luminance area for multiple arcs in OP pattern is much larger than that in AD pattern. The fluctuation degree of arc spatial distribution both in AD and OP patterns is relatively small in the central area of the the arc chamber. Therefore, the parameter of electrode arrangements can provide new consideration for further arc generator design.

The effect of electrode arrangement on the size of arc luminance area provides valuable guidelines for the spheroidization performance of silica powders. The spheroidization rate of $SiO_2$ increases by at least 20% in OP pattern than that in AD pattern under the same experimental conditions. Furthermore, the spheroidization rate of $SiO_2$ can also be enhanced by increasing the discharge power.

## References


[1] Osterhouse D J, Lindsay J W and Heberlein J V R 2013 *J. Phys. D: Appl. Phys.* **46** 224013
[2] Kavka T, Chumak O, Šonsky J, Heinrich M, Stehrer T and Pauser H 2013 *J. Phys. D: Appl. Phys.* **46** 065202
[3] Pakseresht A H, Rahimipour M R, Vaezi M R and Salehi M 2016 *Mater. Chem. Phys.* **173** 395
[4] Kumar S, Selvarajan V, Padmanabhan P V A and Sreekumar K P 2006 *J. Mater. Process. Technol.* **176** 87
[5] Pershin L, Mitrasinovic A and Mostaghimi J 2013 *J. Phys. D: Appl. Phys.* **46** 224019
[6] Bobzin K, Kopp N, Warda T, Petković I, Zimmermann S, Hartz-Behrend K, Landes K, Forster G, Kirner S, Marqués J L, Schein J, Prehm J, Móhwald K and Bach F W 2013 *J. Thermal Spray Technol.* **22** 502
[7] Liu T, Ansar A and Arnold J 2017 *Plasma Chem. Plasma Process.* **37** 1009
[8] Wang F, Cressault Y, Teulet P, Li H and Yang K 2019 *Plasma Chem. Plasma Process.* **39** 1049
[9] Perna A, Minutillo M, Lubrano Lavadera A and Jannelli E 2018 *Waste Manag.* **73** 424
[10] Liang F, Tanaka M, Choi S and Watanabe T 2017 *Carbon* **117** 100
[11] Lei P, Boies A M, Calder S and Girshick S L 2012 *Plasma Chem. Plasma Process.* **32** 519
[12] Poritskii P V 2006 *High Temperature* **44** 328
[13] Lowke J J 1970 *J. Appl. Phys.* **41** 2588
[14] Wang L L, Lu F G, Wang H P, Murphy A B and Tang X H 2014 *J. Phys. D: Appl. Phys.* **47** 465202
[15] Harry J E and Hobson L 1979 *J. Phys. E: Sci. Instrum.* **12** 357
[16] Harry J E and Hobson L 1979 *IEEE Trans. Plasma Sci.* **7** 157
[17] van der Walt I J, Havenga J L and Nel J T 2008 *IEEE 35th International Conference on Plasma Science*, June 15–19, 2008, Karlsruhe, Germany, p. 1
[18] Chen L W, Meng Y D, Shen J, Shu X S, Fang S D and Xiong X Y 2009 *J. Phys. D: Appl. Phys.* **42** 055505
[19] Yao Y, Hossain M M, Watanabe T, Matsuura T, Funabiki F and Yano T 2008 *Chem. Engin. J.* **139** 390
[20] Liu Y, Tanaka M, Choi S and Watanabe T 2014 *Int. J. Appl. Glass Sci.* **5** 443
[21] Watanabe T, Liu Y and Tanaka M 2014 *Plasma Chem. Plasma Process.* **34** 443
[22] Schein J, Zierhut J, Dzulko M, Forster G and Landes K D 2007 *Contrib. Plasma Phys.* **47** 498
[23] Zhang D Q, Zheng L L, Hu X Y and Zhang H 2016 *Int. J. Heat. Mass. Tranaform.* **98** 508
[24] Wang C, Cui H-C, Li W-W, Liao M-R, Xia W-L and Xia W-D 2017 *Chin. Phys. B* **26** 025202
[25] Wang C, Zhang Z, Xia W, Cui H and Xia W 2017 *Plasma Chem. Plasma Process.* **37** 371

[26] Rehmet C, Rohani V, Cauneau F and Fulcheri L 2013 *Plasma Chem. Plasma Process.* **33** 491

[27] Rehmet C, Fabry F, Rohani V, Cauneau F and Fulcheri L 2013 *Plasma Chem. Plasma Process.* **33** 779

[28] Collares M P and Pfender E 1997 *IEEE Trans. Plasma Sci.* **25** 864

[29] Eckert E R G, Pfender E and Wutzke S A 1968 *AIAA J.* **6** 1474

[30] Rat V, Mavier F and Coudert J F 2017 *Plasma Chem. Plasma Process.* **37** 549

[31] Tu X, Yan J, Yu L, Cen K and Cheron B 2007 *Appl. Phys. Lett.* **91** 131501

[32] Coudert J F, Planche M P and Fauchais P 1995 *Plasma Chem. Plasma Process.* **16** S211

[33] Duan Z and Heberlein J 2002 *J. Thermal Spray Technol.* **11** 44

[34] Takana H, Jang J, Igawa J, Nakajima T, Solonenko O P and Nishiyama H 2010 *J. Thermal Spray Technol.* **20** 432

[35] Chumak O, Kavka T and Hrabovsky M 2008 *IEEE Trans. Plasma Sci.* **36** 1062

[36] Yao Y, Yatsuda K, Watanabe T, Matsuura T and Yano T 2009 *Plasma Chem. Plasma Process.* **29** 333

[37] Ghiyasiyan-Arani M, Masjedi-Arani M and Salavati-Niasari M 2016 *J. Mater. Sci.: Mater. Electron.* **27** 4871